

Decentralized Cooperative Control of Multiple Energy Storage Systems in Urban Railway Based on Multiagent Deep Reinforcement Learning

Feiqin Zhu¹, Student Member, IEEE, Zhongping Yang¹, Member, IEEE, Fei Lin¹, Member, IEEE, and Yue Xin, Student Member, IEEE

Abstract—Nowadays, the stationary energy storage systems (ESSs) are widely introduced to recover the regenerative braking energy in urban rail systems. And the multiple ESSs along the line, substations, traction, and braking trains in the traction power system make up a multienergy coupling system, whose energy efficiency is expected to be improved. With the aim of power flow optimization, a cooperative control strategy for multiple ESSs based on multiagent deep reinforcement learning is proposed in this article. Under the distributed control structure, the decision process of multiple ESS agents is formulated as a fully cooperative Markov game, in which each ESS makes independent decision and cooperates to improve the overall energy saving effect. And the value decomposition network, which decomposes the joint state-action value into value functions across agents, is adopted to stabilize the multiagent learning process. Three train operation scenarios are presented in simulation, and the power flow distributions are analyzed quantitatively to better evaluate the performance of the proposed cooperative strategy. A power hardware-in-the-loop (PHIL) experimental platform, which integrates the RT-LAB simulator and physical supercapacitor-based energy storage system (SCESS) is developed in this article to emulate the dc traction power system with multitrain operation. Based on the PHIL platform, the proposed cooperative control strategy is implemented experimentally. Both simulation and experimental results show that in comparison with genetic algorithm (GA), the proposed strategy optimizes the energy distribution between different SCESSs and trains, and improves the overall energy saving effect of the multi-SCESSs.

Index Terms—Cooperative control, energy storage system (ESS), multiagent reinforcement learning (RL), power hardware-in-the-loop (PHIL), urban railway.

I. INTRODUCTION

WITH the increasing demand of energy saving and emission reduction, systematic energy consumption reduction of the urban rail systems has been drawing increasingly attention. At present, the regenerative braking is widely used, and the regenerative energy is considerable due to frequent

Manuscript received August 27, 2019; revised December 26, 2019; accepted January 23, 2020. Date of publication February 4, 2020; date of current version May 1, 2020. This work was supported by the National Key R&D Program of China under Grant 2017YFB1201105. Recommended for publication by Associate Editor F. W. Fuchs. (*Corresponding author: Feiqin Zhu*)

The authors are with the School of Electrical Engineering, Beijing Jiaotong University, Beijing 100044, China (e-mail: 15117405@bjtu.edu.cn; zhpyang@bjtu.edu.cn; flin@bjtu.edu.cn; 17121512@bjtu.edu.cn).

Color versions of one or more of the figures in this article are available online at <https://ieeexplore.ieee.org>.

Digital Object Identifier 10.1109/TPEL.2020.2971637

starts and stops of urban rail trains [1]. However, if there are no energy consumption loads, such as adjacent traction trains, the pantograph voltage will rise rapidly, causing the intervention of braking resistor. Therefore, the utilization of regenerative braking energy is essential to energy saving in urban rail system, and several braking energy recovery technologies are investigated by the researchers, including train operation optimization, reversible substations, and the energy storage system (ESSs) [2]. For the train operation optimization, the train operation curves as well as the train diagrams are adjusted to increase the overlap time of powering and braking trains, so that more regenerative braking energy is directly utilized by the powering trains [3]. It requires no additional investment costs, but is strictly restricted by train operating constraints, such as punctuality and tracking intervals. The reversible substations feed the braking energy to the ac grid, it achieves good energy saving effect, however, as the converter is interfaced with the ac grid, the power shocks and harmonic pollution should be fully considered. For the ESSs, the regenerative braking energy is stored in the ESS and released later for the powering trains. Therefore, the energy circulates inside the traction power supply system, and the ESSs are also capable of suppressing network voltage fluctuation and reducing peak powers of substations [4]. The supercapacitor (SC) has advantages of high power density and long cycle life, thus matches well with the train's high, instantaneous, and frequent braking power [5]; effective braking energy recovery of SC-based ESS (SCESS) has been demonstrated in field tests of several metro lines around the world [6], [7].

The control strategy of ESS determines the working states and charge/discharge currents of ESS under different system states, thus is responsible for state of charge (SOC) management and deployment of regenerative braking energy distribution. It is critical to optimize the control strategy, maximize the utilization of ESS capacity, and realize optimal power dispatch of the traction power system [8], [9]. The line-voltage control strategy determines the working mode on the basis of network voltage [10]–[12], which is most widely used in SCESSs that have been installed in actual metro systems. However, current research on control strategies mainly focuses on the performance of a single SCESS. With the development of energy storage technologies, installing multiple SCESSs along the whole metro line will be the trend. In that case, energy interaction between the SCESSs, the rectifier units in substations, and the powering/braking trains

is synthetically influenced by the control parameters of different SCESs [13], [14]. Therefore, for purpose of improving the overall energy saving effect of the SCESs, it is necessary to control multiple SCESs cooperatively, considering SOCs of SCESs as well as operating states of trains.

For the cooperative management problem of multienergy system, the evolutionary algorithm was introduced in [15] and [16] to optimize the control parameters offline. However, as a sort of static optimization method [17], the control parameters cannot be adjusted dynamically with respect to the system states. The structure of cooperative control can be mainly classified into two categories, i.e. the centralized control and the decentralized control. The calculation complexity increases dramatically with the number of individuals in the centralized algorithm. For decentralized control, the game theory was applied in energy management of the battery/SC/diesel hybrid system in [18]. The individuals make decisions with respect to their utility functions in a distributed manner. However, the team profit cannot be guaranteed and the efficiency of the equilibrium point should be further enhanced in the noncooperative game. The sequential decision making problem of multiple individuals is solved by differential game theory in [19]. However, for the traction power system, which consists of multiple nonlinear energy sources and consumption loads, and has a time-variant topology due to movement of trains, the model complexity makes it hard to obtain the theoretical optimal cooperative strategy. In [20], a cyber–physical–social system (CPS) was established to realize optimal power dispatch in the power grid system. Learned from the concept of CPS, it is significant to utilize the artificial intelligence and communication technologies to manage the power flow, and improve the overall energy efficiency of the traction power system. At present, data communication system has been widely used in communication-based train control systems for urban rail transit. It transmits the train information to the ground automatic train supervision (ATS), zone controller (ZC) etc., so ATS and ZC implement monitoring of train operation, send movement authority, and operation instructions to the trains. Research works on the communication-based train operation optimization have also been conducted by scholars. Su *et al.* proposed a cooperative control model that effectively utilizes the regenerative energy of braking trains by adjusting the departure time of accelerating trains [21]; an energy-efficient train operation optimization algorithm based on real-time traffic information was developed in [22]. Therefore, benefiting from the rapid development of communication technologies, it is realizable to obtain the states of trains, ESSs, and substations in real time, and, then, adjust parameters of the ESSs dynamically.

Recently, deep reinforcement learning (DRL) has demonstrated to be effective to deal with complex control problem [23]–[25]. A lot of work has been conducted to extend the DRL algorithms to multiagent systems (MASs) [26]–[28]. However, the key challenge for multiagent DRL (MADRL) is that the system environment is no longer stationary from the perspective of the individual agents, as multiple agents learn simultaneously and interact with the environment as well as each other. In order to tackle with the nonstationary problem, the fingerprints, which contained information about the age of

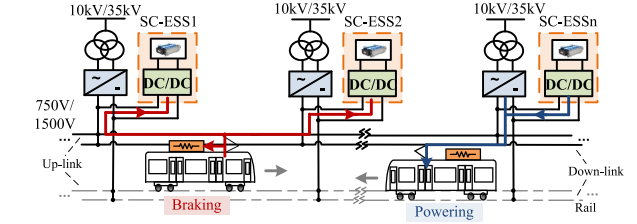


Fig. 1. Systematic diagram of the traction power system with multiple SCESs in urban railway.

data, was added to the training samples in [29]. In [30], the multiagent deep deterministic policy gradient was proposed for mixed cooperative-competitive environment, which stabilizes the training process by inferring the policies of other agents. In [31], a value decomposition network (VDN) was deduced for fully cooperative MAS, in which the joint action-value function was decomposed into local value functions across agents. With the aim of minimizing the total energy consumption of the traction power system, this article develops a decentralized cooperative control strategy for multiple SCESs based on VDN. The “centralized training, decentralized execution” architecture is employed to avoid nonstationarity: in the training stage, parameters of Q-networks are updated by minimizing the loss function of the team Q-network; and in the execution stage, each agent obtains local observations, makes independent decisions based on the local Q-network, and performs the actions with the line-voltage-based hierarchical control structure. Under the proposed strategy and the genetic algorithm (GA)-based strategy, the power flow distributions in several train operation scenarios are quantitatively analyzed, and the system energy efficiency is evaluated in terms of braking energy feedback rate, transmission efficiency, and energy saving rate. Furthermore, a power hardware-in-the-loop (PHIL) experimental platform is developed and the proposed cooperative strategy is verified experimentally: the dc traction power system is emulated by the RT-LAB real-time simulator (RLS), and it realizes cooperation with the physical SCES through the power amplifier.

The remainder of this article is organized as follows. In Section II, the mathematical models of trains and ESSs are established, and the energy interaction of the traction power system is exhibited; in Section III, the cooperative Markov game (MG) and the VDN is introduced, based on which the cooperative control strategy is proposed; simulation studies based on specific metro line are presented in Section IV, and control strategies are compared in terms of braking energy feedback rate, transmission efficiency, and energy saving rate; in Section V, the proposed strategy is verified with the PHIL experimental platform.

II. MATHEMATICAL MODEL OF THE TRACTION POWER SYSTEM

Fig. 1 shows the systematic diagram of the traction power system with multi-SCESs. The SCESs are installed in different substations along the metro line. The trains are equipped with onboard braking resistors, which consume the braking energy to prevent over voltage. Therefore, the substation rectifiers,

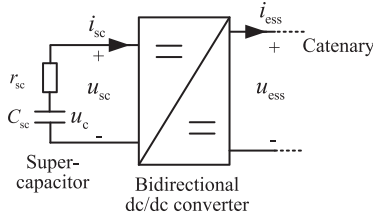


Fig. 2. SC-based ESS.

charging/discharging SCESs, powering/braking trains, and braking resistors act as either energy consumers or consumption loads, performing complex energy interactions. In this section, mathematic model of each component is established, and evaluations for the system energy flow are introduced.

The kinematics equation of the train in a discrete-time form is formulated as

$$\begin{cases} a = (F_t - w(v) - g(x)) / Mg \\ v(t + \Delta t) = v(t) + a \cdot \Delta t \\ x(t + \Delta t) = x(t) + [v(t + \Delta t) + v(t)] / 2 \cdot \Delta t \end{cases} \quad (1)$$

where a is the acceleration rate, F_t denotes the traction/braking force of the motors, and $w(v)$ represents the basic resistance of train, which is calculated by the Davis equation [22]. $g(x)$ represents the additional resistance, including the gradient resistance, the curve resistance, etc., v and x , respectively, denote the train velocity and displacement.

Based on the train's dynamic model, the power, velocity, and displacement at each moment are calculated with the fixed-time algorithm, which derives the train operation given the running time and speed constraints of each line section [32]. And in the equivalent circuit model of dc traction power system, the train is modeled as a controlled power source, which absorbs power from the traction network when powering, and releases energy back when braking.

The SCESS consists of the bidirectional dc–dc converter and the SC modules, as seen in Fig. 2. The dc–dc converter implements voltage conversion between SC and the catenary and manages the charge/discharge current of SC. The SC is modeled as a voltage source in series with the equivalent internal resistance. The dynamic equation of the SC is expressed as

$$\begin{cases} u_c(t + \Delta t) = u_c(t) + i_{sc}/C_{sc} \cdot \Delta t \\ u_{sc}(t) = u_c(t) + r_{sc} \cdot i_{sc} \end{cases} \quad (2)$$

where u_{sc} and i_{sc} are voltage and current of SC.

The power balance equations of two sides of the dc–dc converter is formulated as

$$u_{ess} \cdot i_{ess} = \begin{cases} (u_{sc} \cdot i_{sc}) \cdot \eta_{dc/dc}, \text{ discharge} \\ (u_{sc} \cdot i_{sc}) / \eta_{dc/dc}, \text{ charge} \end{cases} \quad (3)$$

where u_{ess} and i_{ess} , respectively, represent the voltage and current at the catenary side and $\eta_{dc/dc}$ is the efficiency of dc–dc converter.

Fig. 3 presents the energy flow between the energy sources and loads. It is seen that the total energy consumption can be minimized by increasing energy recycling and reducing energy

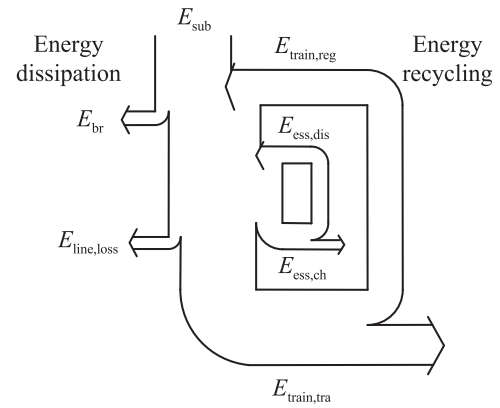


Fig. 3. Diagram of energy flow in the traction power system.

dissipation on braking resistors and line resistance. Three evaluation indexes are formulated to better evaluate the energy flow distribution of the traction power system, as seen in (4), (5), and (6), respectively. r is defined as the ratio of braking energy that feedback to the grid, to the total braking energy of trains. It evaluates the proportion of regenerative energy that is available to the powering trains and the ESSs. The larger r is, the higher receptivity of the power network will be. η is calculated by the ratio of traction energy consumption to the total energy that is provided to the power network. It quantizes the energy transmission efficiency between substations, trains, and ESSs, and will be improved by minimizing the energy loss during transmission. e is the energy saving rate of the ESSs. It is formulated as the ratio of change of substation energy consumption after installing ESSs to the total energy consumption without ESSs. Therefore, e measures the effect of ESSs on energy consumption reduction

$$r = \left(1 - \frac{E_{br}}{E_{reg}} \right) \times 100\% \quad (4)$$

$$\eta = \frac{E_{tra}}{E_{sub} + (E_{reg} - E_{br}) - \Delta E_{sc}} \times 100\% \quad (5)$$

$$e = \left(1 - \frac{E_{sub}}{E_{noess}} \right) \times 100\% \quad (6)$$

where E_{sub} represents the total energy consumption of substations after installing ESSs, and E_{sub}^{noess} denotes the total substation output energy without ESSs. $E_{train,tra}$ and $E_{train,reg}$, respectively, denote the traction and regenerative energy of the trains, E_{br} represents the energy dissipation on braking resistors, $E_{line,loss}$ is the line transmission loss, $E_{ess,ch}$ and $E_{ess,dis}$ are charge/discharge energy of ESS, and ΔE_{sc} is the change of stored energy in the SC.

III. COOPERATIVE CONTROL BASED ON MADRL

In this article, the MADRL technology is employed to implement cooperative control of multi-SCESSs in the urban rail system. This section presents a detailed description about the fully cooperative decision model of multi-SCESSs, and introduces the MAS-based holistic learning framework as well as the hierarchical controller of individual SCESS.

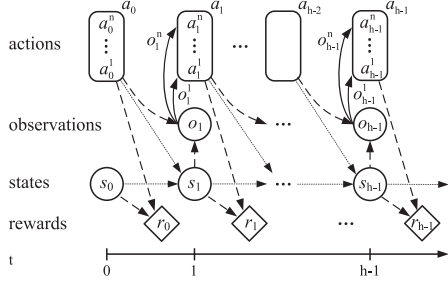


Fig. 4. Block diagram of Dec-POMDP.

A. Cooperative MG

The decision process for the MAS is regarded as an MG [33], which is an extension of the Markov decision process (MDP), as seen in (7). The state transition and reward generated by the environment is determined by the joint action of all the agents. In this article, the state transition is based on the dynamics of the trains and SCESs, as seen in (1) and (2), respectively, and is realized in the traction power system simulator. According to the cooperation degree between agents, the MGs are classified into fully cooperative, fully competitive, and mixed MGs. For the fully cooperative MG, agents cooperate to achieve a common goal, they share the same reward function, and the fully cooperative MG is also considered as a decentralized partially observable MDP (Dec-POMDP), as seen in Fig. 4 [34]. In this article, SCESs in different substations cooperate to improve the overall energy saving effect, thus the Dec-POMDP is adopted to model the decision process for multi-SCESs

$$\langle m, S, A^{(1)}, \dots, A^{(m)}, T, R^{(1)}, \dots, R^{(m)} \rangle \quad (7)$$

where m is the number of agents, S is the set of states, $A^{(i)}$ is the action space of agent i , $T : S \times A \times S \mapsto [0, 1]$ is the state transition probability function, and $R^{(i)} : S \times A \mapsto \mathbb{R}$ is the reward function for agent i .

B. Value Decomposition Network

Reinforcement learning (RL) consists in learning the policy that maximizes the long-term return by interacting with the environment. The deep Q learning is a representative RL algorithm that improves the policy by value iteration, and approximates the state-action value with a deep neural network to avoid the curse of dimensionality. The state-action value [denoted as $Q^\pi(s, a)$], is defined as (8), it is the expected return when the agent lies in state s , takes the action a , and, thereafter, follows policy π . However, independent Q learning (IQL) in MAS faces the nonstationary problem as the dynamics of the environment is affected by the change of teammates' policies. In order to stabilize the concurrent learning process, a VDN was proposed in [31] for cooperative MG. The joint action-value function Q_{tot} of multiple agents is approximated by the sum of individual Q functions for each agent, as seen in (9). h_i is the history of observation for agent i . Therefore, improvement of Q_{tot} contributes to the increase of local Q-values. And the algorithm complexity increases linearly with the number of agents, instead of increasing exponentially

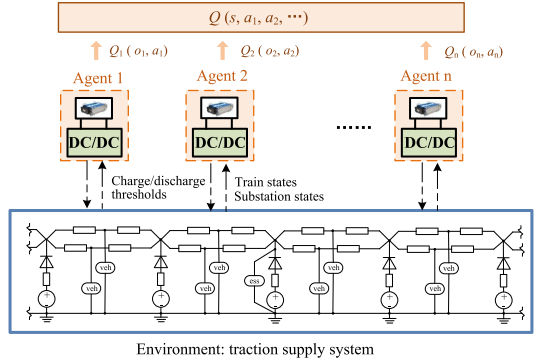


Fig. 5. Framework of cooperative control strategy for multi-SCESs based on MAS.

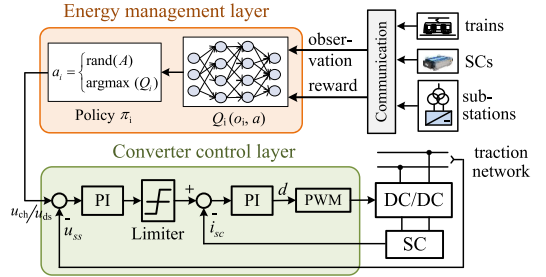


Fig. 6. Hierarchical control structure for individual SCESS.

in a centralized control structure. VDN adopts the mechanism of “centralized training, decentralized execution.” In the training phase, parameters of Q-functions are updated by minimizing the loss function with respect to Q_{tot} , as seen in (10). And in the execution phase, each agent obtains local observations, and performs ε -greedy action selection [as seen in (11)], according to the local Q-function, which implements distributed decision making and helps reduce the communication requirement

$$Q^\pi(s, a) = \mathbb{E} \left[\sum_{t=1}^{\infty} \gamma^{t-1} r(s_t, a_t) | s_1 = s, a_1 = a; \pi \right] \quad (8)$$

$$Q_{\text{tot}}(h, a) \approx \sum_{i=1}^n Q_i(h_i, a_i; \theta_i) \quad (9)$$

$$L(\theta) = \frac{1}{b} \sum_{j=1}^b (y_j^{\text{tot}} - Q_{\text{tot}}(h, a; \theta))^2 \quad (10)$$

where $y_j^{\text{tot}} = r_j + \gamma \max_a Q_{\text{tot}}(h, a; \theta^-)$ is the target value of Q_{tot} , γ is the discount factor, b is the mini-batch size, θ^- and θ , respectively, denote the parameters of target network and value network

$$a_i = \begin{cases} \text{argmax}_i Q_i(h_i, a_i), \text{rand}(1) \leq 1-\varepsilon \\ \text{rand}(A), \text{otherwise.} \end{cases} \quad (11)$$

C. VDN-Based Cooperative Learning Strategy (VCLS)

Fig. 5 presents the framework of proposed cooperative control strategy based on MAS, and Fig. 6 shows the hierarchical control

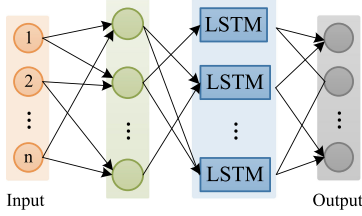


Fig. 7. Structure of local Q-network for each agent.

structure for individual SCESS. Each SCESS is modeled as an intelligent agent and the traction power system is regarded as the environment. In the energy management layer, the SC agent obtains local observations through communication system, makes independent decision with respect to the local Q-network, and the parameters of the Q-networks are updated by performing gradient descent on Q_{tot} during the training process. In this article, the observation for each agent is defined as (12), including the powers and displacements of trains that locate at the adjacent feeding sections, and SOCs of SCESSs in neighboring substations. The structure of local Q-network is depicted in Fig. 7. It consists of an input layer, a fully connected layer, a long short-term memory (LSTM) layer, and an output layer, which respectively contains 10, 16, 8, and 4 units. The decentralized control architecture and approximation of Q-values by the neural network help in avoiding the curse of dimensionality. The action generated by the ε -greedy policy is sent to the converter control layer, which tracks the instruction of the energy management layer by adjusting the IGBT driving pulses of the dc–dc converter

$$o_i = [d_{ki}, p_{ki}, \text{soc}_i, \text{soc}_{ji}] . \quad (12)$$

The proposed cooperative algorithm is on the basis of the line-voltage-based control scheme, where the SCESS charges to stabilize the network voltage at the charge voltage threshold when trains are braking, and discharges to keep the network voltage at the discharge voltage threshold when trains are powering. Therefore, the action for agent i is represented as (13), and the charge/discharge thresholds are adjusted in real time

$$a^{(i)} = [u_{\text{ch}}, u_{\text{dis}}] \quad (13)$$

where u_{ch} and u_{dis} , respectively, denote the charge threshold and the discharge threshold for SCESS.

In the fully cooperative multiagent learning, the agents share the team reward function r , which evaluates the joint action of all agents. In this article, r is formulated as (14). It includes the normalized increment of energy consumption of the substations in each time step Δt as well as the normalized increment of energy dissipation on braking resistors. Therefore, both increase of substation output energy and the braking resistor loss will be punished

$$\begin{aligned} r = c - \sum_{i=1}^n \int_t^{t+\Delta t} i_{\text{ss},i} \cdot u_{\text{ss},i} d\tau / E_{\text{nom}} \\ - \sum_{j=1}^m \int_t^{t+\Delta t} i_{\text{br},j} \cdot u_{\text{t},j} d\tau / E_{\text{nom}} \end{aligned} \quad (14)$$

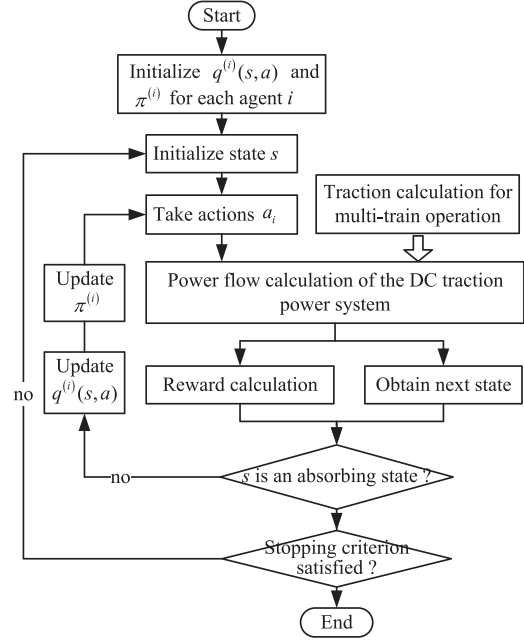


Fig. 8. Flowchart of the learning process.

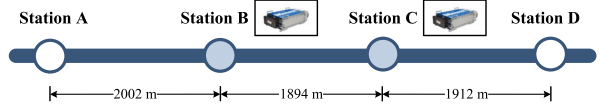


Fig. 9. Metro line section for simulation.

where c is the reward bias, and E_{nom} represents the energy benchmark, which is calculated by the total energy consumption of substations without SCESSs.

The flowchart of the learning process of the proposed cooperative control strategy is shown in Fig. 8. First, the individual Q-network, policy for each agent, and the environment states are initialized. Each agent takes an action according to the current policy. The system dynamics is solved with power flow calculation of the dc traction power system and simulation of multitrain operation, which are based on mathematical models established in Section II. Then, the system transfers to the next state, and the agents receives the corresponding reward signal. If the new state is nonterminal, the agents update the Q-networks by minimizing the loss function as seen in (10); otherwise, an episode is finished and the environment state will be reinitialized. The policy of each agent gets improved through the process of iteratively learning.

IV. SIMULATION STUDIES

A. Simulation Conditions

In this section, case studies are presented to verify the overall energy-saving effect of the proposed cooperative control strategy. The metro line section for simulation is depicted in Fig. 9. It contains four substations, two SCESSs, which are, respectively, installed in substations B and C, and several trains following headway of 300 s. It is representative to analyze the power

TABLE I
SIMULATION PARAMETERS

Parameters	Values	Unit
Train set	3M3T	-
Weight (AW2)	279.6	t
Traction notch	4	-
Braking notch	3	-
Starting voltage of braking resistor	900	V
Substation no-load voltage	860	V
Substation internal resistance	0.0161	Ω
Catenary unit resistance	0.0191	Ω/km
Rail unit resistance	0.017	Ω/km
Supercapacitor module name	BMOD0063 P125	-
Connections	17P5S	-
Permissible voltage range	312.5–593.0	V
Efficiency of dc/dc converter	0.98	-

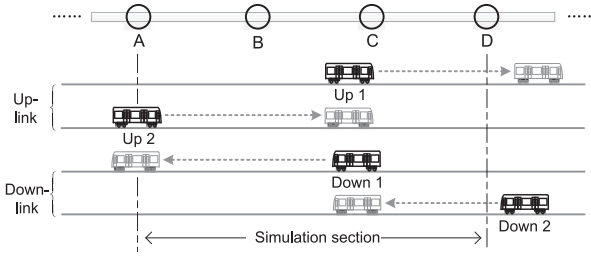


Fig. 10. Diagram of train moving process.

flow between the trains, substations, and ESSs. The simulation parameters are listed in Table I. The rated power of each SCESS is 1.5 MW, and the total stored energy is 11.6 kWh. The SOC range of SC is 0.25–0.9, and the initial SOC is set at 0.27 in simulation.

Fig. 10 shows the moving process of the trains during one headway of 300 s. The first train of uplink (denoted as Up1) is braking near station C and the first train of downlink (denoted as Down1) is cruising initially. They leave the line section successively, and the next trains of uplink and downlink, respectively, come into the section from stations A and D. The power curves and displacement curves of the trains are depicted in Fig. 11(a)–(d). The trains accelerate with traction notch 4 (acceleration rate 0.905 m/s²), and decelerate with braking notch 3 (deceleration rate 0.34 m/s²). The maximum traction power is 3.7 MW, and the maximum braking power is 2 MW.

B. Algorithm Performance

Fig. 12 compares the iteration curves under IQL with fully connected network, IQL with LSTM network (IQRL), and the VCLS. In order to have a fair comparison, the algorithm parameters are set equally. The training parameters of the algorithms are listed in Table II. It is observed that the mean episode reward under IQL with fully connected network gets little improved, as the independent exploration of different agents makes it hard for the agents to learn a policy stably. The performance of IQRL is better than that of IQL, this may be because the recurrent nature

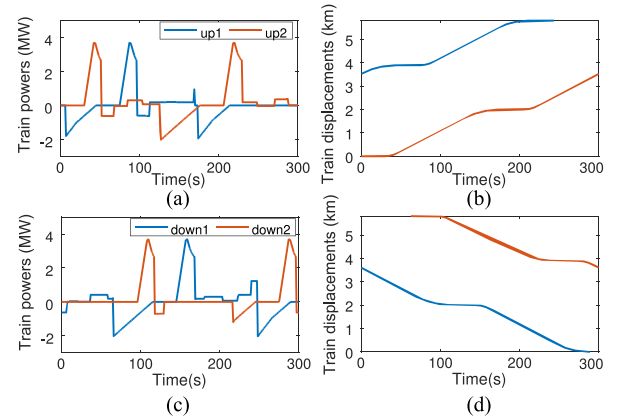


Fig. 11. Operating curves of trains in one headway.

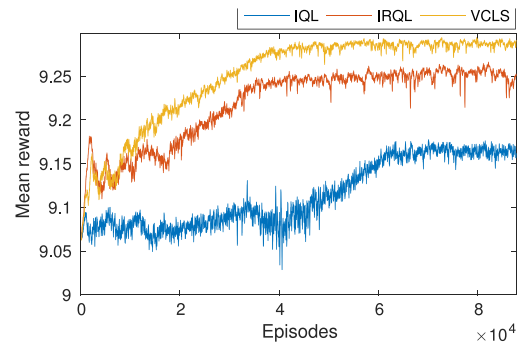


Fig. 12. Training curves of algorithms.

TABLE II
TRAINING PARAMETERS OF THE ALGORITHMS

Parameters	Values	Parameters	Values
Learning rate	10^{-3}	Replay buffer size	10^6
Batch size	32	Target update frequency	5000

of LSTM network helps in predicting the change of environment dynamics. Under the VCLS, the mean episode reward is further improved in comparison with that of IQRL, it validates VCLS realizes stable training and obtains the best performance with cooperation of different agents.

C. Scenario Analysis

For comparison, the genetic optimization (GA) is employed to optimize the voltage thresholds of the constant-threshold strategy, it is a type of heuristic stochastic optimization algorithm and has been used in a number of literatures to optimize the control parameters of ESSs [35]–[37]. The chromosome (also known as the individual) represents a design point for the system. In this article, it is defined as the charge and discharge thresholds of the ESSs with real-number encoding, i.e., $x_i = [u_{\text{ch}}, u_{\text{dis}}]$, where u_{ch} and u_{dis} are the genes of chromosome. The population is the set of all the individuals in one generation. The fitness function evaluates the goodness of each individual, and is defined as (15) in this article. The objective function is the sum

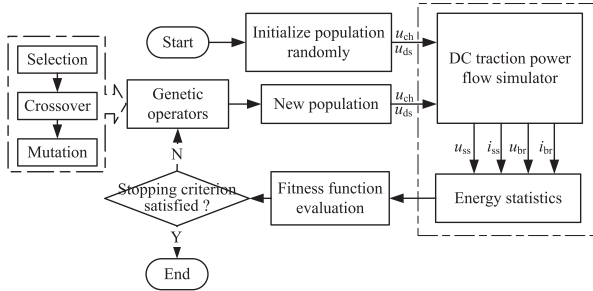


Fig. 13. Optimization process of GA.

TABLE III
OPTIMIZATION PARAMETERS OF GA

Parameters	Values	Parameters	Values
Population size	50	Crossover fraction	0.7
Mutation fraction	0.05	Maximum generations	50

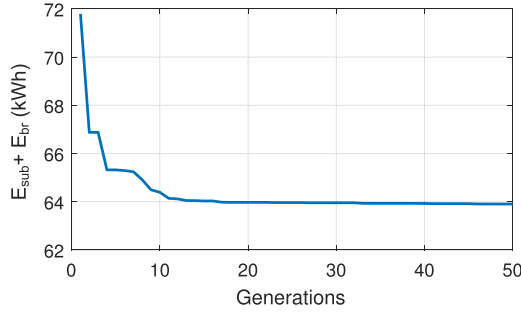


Fig. 14. Evolution curve of GA.

of energy consumptions of substations and braking resistors in one headway, and the ranking function maps the objective to the fitness according to the decreasing order [38]. The optimization algorithm selects the individuals that reproduce new generations based on their fitness function values. In this article, the probability of each individual selected is in proportionally to its fitness, as seen in (16). The optimization process of GA is presented in Fig. 13: the dc traction power simulator performs power flow calculation for one headway to obtain the fitness functions, and the genetic operators are executed to produce new individuals with improved fitness. The algorithm parameters of GA are listed in Table III, and Fig. 14 shows the evolution curve. It is observed from Fig. 14 that the energy consumptions get reduced with increase of generation, and converges to 64 kWh after 20 iterations. Thereafter, in this article, GA has good convergence and effectively finds the optimized voltage thresholds. The optimization results are obtained as $u_{ch,opt} = 882$ V, $u_{dis,opt} = 855$ V. One of the main distinctions between VCLS and GA lies in their optimization models. VCLS aims to optimize the policy of each agent, i.e., the function that maps from observations to actions. The optimization model is a dynamic cooperative game (as formulated in Section III-A), which is sequential and dynamic in nature, and the coordination of different agents is important for the team profit. However, GA aims to find static design parameters that optimize the objective function, which

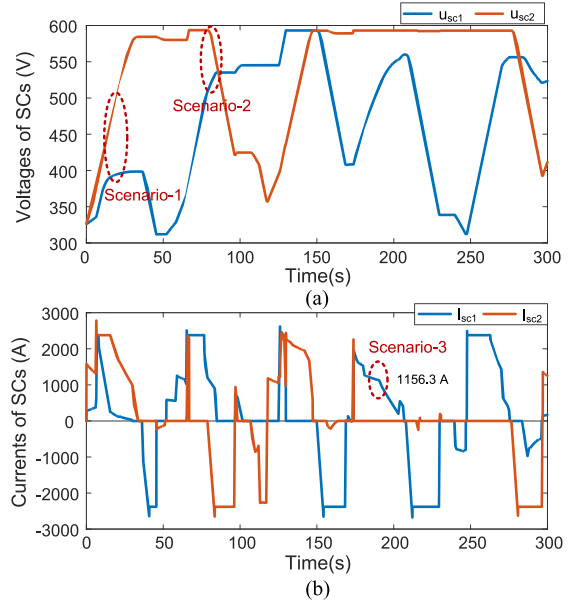


Fig. 15. Operating curves of the two ESSs under GA-based strategy.

belongs to the optimum design problem. The design parameters remain fixed for its entire life [17]. It is noticed from Figs. 12 and 14 that the training process of VCLS is longer than that of GA, this is because for VCLS, the Q-networks that maps from observations to action evaluation values are trained, which have much more parameters than those in GA (only the static charge and discharge voltage thresholds are optimized). The optimization process of GA is conducted offline, the optimized parameters are stored in the controller, and employed directly for real-time execution. The implementation processes of VCLS includes the training stage and execution stage. VCLS learns the parameters of the local Q-network in the pretrain stage; during the execution stage, it samples the system states in each time step (1 s in this article), calculates the Q-networks in real time with the trained parameters and current observations, and performs action selection with respect to (11). Specifically, the computation time of VCLS execution stage is around 0.52 ms on a personal computer (PC) with a CPU of 2.3 GHZ, which is within the time step

$$F = \text{ranking}(E_{sub} + E_{br}) \quad (15)$$

$$p_i = F_i / \sum_{j=1}^N F_j. \quad (16)$$

Figs. 15 and 16, respectively, present operating curves of the two SCESs under GA-based strategy and VCLS. Fig. 17 depicts the adjustment of voltage thresholds under VCLS. In order to have a more intuitive evaluation of the operation performance under the two strategies, three train operation scenarios within the simulation period are presented and the power distributions under the two strategies are analyzed quantitatively. Fig. 18 shows the train operation during scenario-1 (at 20 s), where the first up-link train is braking near station C, and the first down-link train is cruising. Current distributions of the system under the

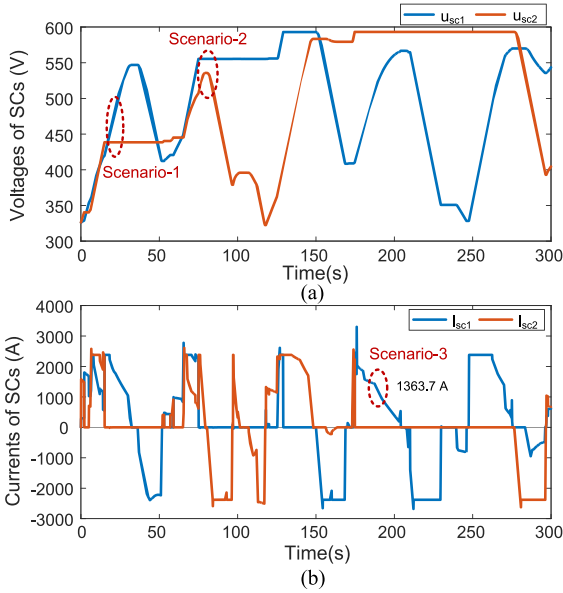


Fig. 16. Operating curves of the two ESSs under VCLS.

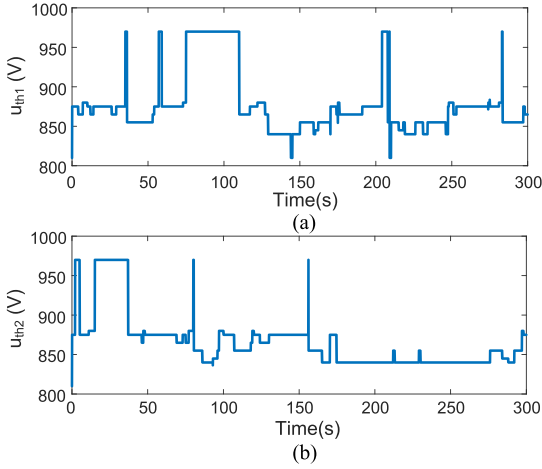


Fig. 17. Voltage thresholds adjustment curves of the two ESSs.

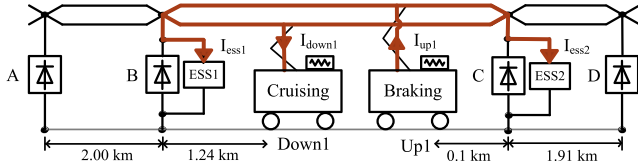


Fig. 18. Diagram of train operation during scenario-1.

two strategies are compared in Table IV. Under the GA-based strategy, the braking energy distribution is passively determined by the train states: as the distance between the braking train and the ESS2 is shorter, ESS2 charges with a larger current of 1047.7 A at traction network side, and the SC voltage rises rapidly to 584.5 V at 34 s, while the charging current of ESS1 is merely 61.7 A (at catenary side). However, under VCLS, the distribution of braking energy is changed obviously by adjustment of the voltage thresholds: voltage of SC1 rises to 547 V

TABLE IV
CURRENT DISTRIBUTION OF THE SYSTEM IN SCENARIO-1

Currents	I_{up1} (A)	I_{down1} (A)	I_{ess1} (A)	I_{ess2} (A)
GA	1148.1	38.7	61.7	1047.7
VCLS	1115.6	38.0	1077.6	0

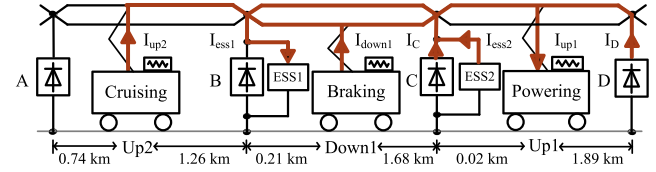


Fig. 19. Diagram of train operation during scenario-2.

TABLE V
CURRENT DISTRIBUTION OF SCENARIO-2

Currents	GA	VCLS	Currents	GA	VCLS
I_{up2} (A)	38.5	37.5	I_{ess1} (A)	669.6	0
I_{down1} (A)	1615.2	1577.7	I_{ess2} (A)	454.2	0
I_{up1} (A)	1865.1	1860.2	I_C (A)	316.2	178.0
-	-	-	I_D (A)	110.5	66.65

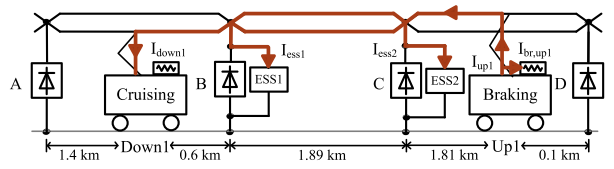


Fig. 20. Diagram of train operation during scenario-3.

and voltage of SC2 rises to 438.6 V. Therefore, in subsequent time interval 68–75 s, under GA-based strategy, the regenerative energy is solely recovered by ESS1, and ESS2 exits working; while under VCLS, the two ESSs charge simultaneously so as to match with the train's braking power. This signifies the proportion of braking energy recovery between different ESSs is optimized under the VCLS, and energy dissipation on braking resistor is effectively reduced.

Fig. 19 shows the power flow of scenario-2, and Table V presents the current distribution of the system under the two strategies. The first train of uplink is accelerating, the first train of downlink is braking, and the second train of uplink is cruising. Under GA-based strategy, the braking energy is recovered by ESS1, while ESS2 discharges to provide traction energy for the first uplink train. However, under VCLS, the voltage thresholds of the two ESSs rise at 970 and 880 V, respectively, thereafter both I_{ess1} and I_{ess2} equal zero, and the braking energy is directly reused by the powering train. Therefore, the proposed VCLS prevents inefficient energy circulation between the two SCESs, and has a better management of SC SOC. Fig. 20 shows the train states and power flow in scenario-3, Table VI lists the current values at different nodes. The first train of uplink is braking near station D. Under GA-based strategy, ESS1 charges with a current of 673.45 A (at catenary side), and the train's braking resistor

TABLE VI
CURRENT DISTRIBUTION IN SCENARIO-3

Currents	GA	VCLS	Currents	GA	VCLS
I_{up1} (A)	1171.5	1178.7	I_{ess1} (A)	673.45	828.15
$I_{br,up1}$ (A)	154.2	0	I_{ess2} (A)	0	0
I_{down1} (A)	343.8	350.6	-	-	-

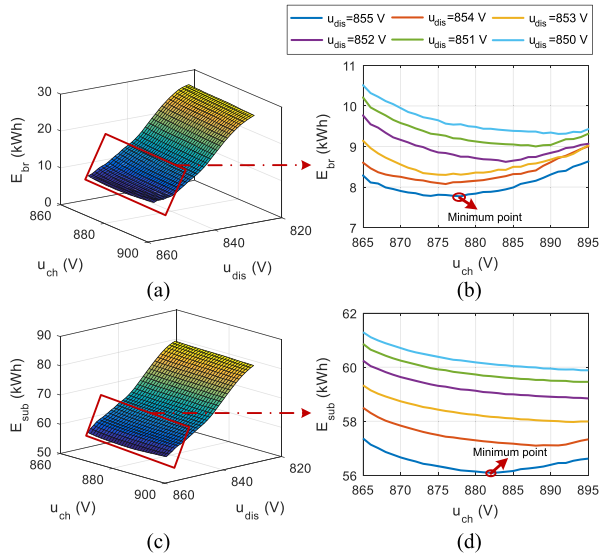


Fig. 21. Relationship between energy consumptions and voltage thresholds under constant-threshold control strategy.

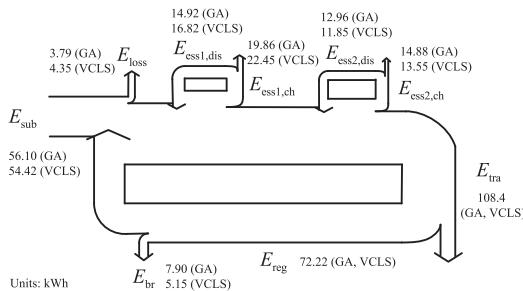


Fig. 22. Energy flow diagram of the system under two strategies.

starts. This is because when the distance between the train and the ESS is far, the line voltage drop is large, thus the pantograph voltage of the train is more likely to exceed the start voltage of braking resistor. However, under VCLS, the voltage thresholds of ESS1 is reduced at 865 V, so the charge current of ESS1 is increased to 828.15 A, and the braking energy is fully recovered. This demonstrates that VCLS adjusts the voltage thresholds dynamically with respect to the train positions, improving the energy transmission between the braking train and the ESSs.

D. Energy Statistics

Fig. 21 shows the relationship between the energy consumptions and the voltage thresholds under constant-threshold control strategy. In Fig. 22, energy flow of the system under GA and VCLS are presented. It is observed from Fig. 21 that E_{br} and

TABLE VII
COMPARISON OF EVALUATION INDEXES UNDER DIFFERENT STRATEGIES

Strategies	$r(\%)$	$\eta(\%)$	$e(\%)$
GA	89.1	95.5	32.1
VCLS	92.9	95.0	34.1

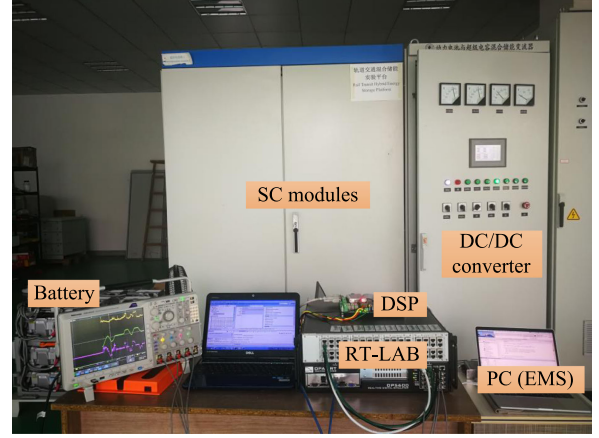


Fig. 23. Photo of PHIL platform for the dc traction power system.

E_{sub} decreases with the increase of u_{dis} , and an inflection point exist with change of u_{ch} . The results of GA ($u_{ch} = 882$ V, $u_{dis} = 855$ V) locates close to the minimum points, validating GA has good performance in heuristic optimization. It is seen from Fig. 22 that under VCLS, the charge energy of ESS1 is increased while less regenerative energy is recovered by ESS2. The energy dissipated on braking resistors and total energy of substations are further reduced by 2.75 and 1.68 kWh respectively in comparison with that of GA. Therefore, VCLS realizes dynamic optimization of the spatial-temporal energy distribution, and improves the energy interaction efficiency of the system more effectively in comparison to the static optimization.

In Table VII, the energy feedback rate r , the transmission efficiency η , and the energy saving rate e defined in Section II [as seen in (4), (5), and (6)] under different strategies are compared. It is seen that under VCLS, r is improved by 3.8% in comparison with that of GA, illustrating that the braking energy is utilized more effectively. Due to the increase of line transmission loss, η is a bit lower in VCLS. However, e of VCLS reaches 34.1%, which is 2.0% higher than that of GA, demonstrating the overall energy saving effect of SCESSs is optimized under VCLS.

V. EXPERIMENTAL VERIFICATION

A. PHIL Experimental Platform

In order to verify the proposed coordinated control strategy, a PHIL experimental platform for dc traction power supply system is developed, as shown in Fig. 23. The experimental platform consists of RT-LAB RLS, physical SC ESS, power amplification module, and energy management system. The configuration of the PHIL platform is shown in Fig. 24. The RT-LAB simulator emulates the operation of the dc traction power system, which consists of multiple trains and substations in real time [39].

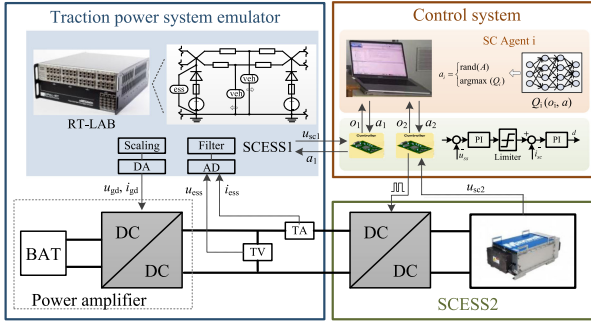


Fig. 24. Configuration diagram of PHL experimental platform.

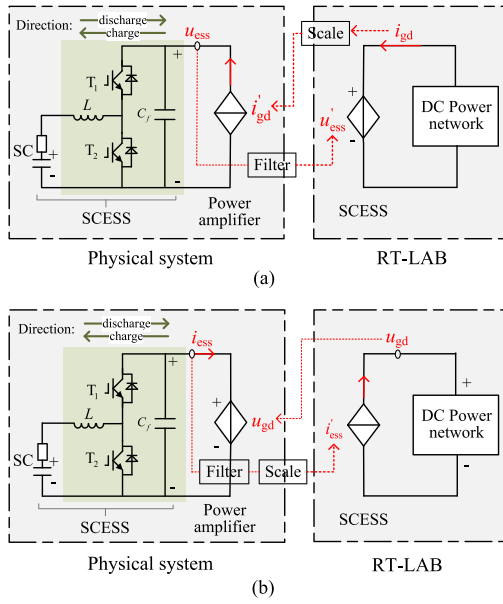


Fig. 25. Control schemes of the power amplifier under two modes.

The trains are modeled as time-variant power sources, and the movement of trains equivalents to the change of line resistance between trains and substations. The parameters of the system are listed in Table I. SCESS1 is emulated in the RT-LAB simulator, and SCESS2 is operating by means of the physical device, including a bidirectional buck/boost converter and SC modules. When SCESS works in charge condition, the dc-dc converter operates as a buck converter, power flows from the dc bus to the SC modules; and when SCESS discharges, it operates as a boost converter, through which the SC modules release energy to dc bus (as seen in Fig. 25). The parameters are presented in Table VIII, the switching frequency of dc-dc converter is 5 kHz in experiment.

The power amplifier consists of a dc power source (the battery pack) and a dc-dc converter. It is the interface between the RLS and the physical system, and implements tracking of the voltage/current signals given by the RT-LAB in energy level. It contains two modes of operation, as seen in Fig. 25(a) and (b): when the current of the SCESS is smaller than the maximum value, the power amplifier acts as a current source, which tracks the scaled network current; when the SCESS current reaches

TABLE VIII
PARAMETERS OF THE PHYSICAL SCESS

Parameters	Values	Unit
Filter capacitance	1	mF
Chopper inductance	1	mH
Switching frequency	5	kHZ
DC bus voltage	750-900	V
Supercapacitor module name	BMOD0063 P125	-
Connections of SC	4S1P	

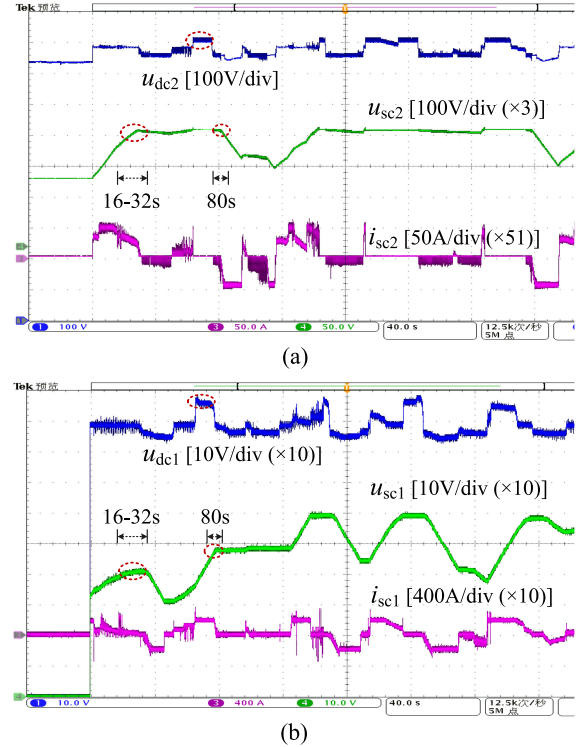


Fig. 26. Experimental operating waveforms of ESSs under GA-based strategy.

the limit, it operates in the voltage source mode, and the voltage instruction equals the network voltage at the high voltage side of the ESS in the RT-LAB simulator. The energy management system consists of a PC and a digital signal processor (DSP) controller. PC implements the cooperative control strategy, and the DSP controller performs the voltage-current double closed-loop control of dc-dc converter. The response time of the voltage controller is within 200 ms, therefore, it realizes good tracking of the instructions of the energy management layer that changes every second.

B. Experimental Results

Figs. 26 and 27, respectively, display the experimental waveforms under the GA-based strategy and VCLS. Figs. 26 and 27(a) are operating waveforms of SCESS2, including the network voltage, SC voltage, and SC current. Figs. 26 and 27(b) are waveforms of SCESS1. Due to the limitation of sampling range of the I/O ports, the sampled values of SCESS1 are scaled with proportion of 1/10. Due to the power and capacity

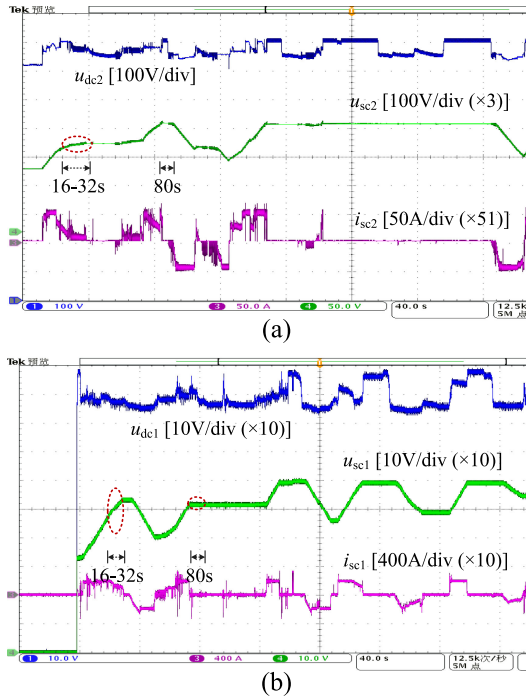


Fig. 27. Experimental operating waveforms of ESSs under VCLS.

limitations of the physical SCESS, the SC current of SCESS2 is reduced by $17 * 3$ times in experiment, and the voltage range of SC is scaled with proportion of 3, so that the power ratio equals the energy ratio of the physical SCESS to that in simulation. It is observed that the experimental waveforms are in consistence with those in simulation. During 16–32 s, the charging current of ESS1 is small, and most of the braking energy is recovered by ESS2 under the GA-based strategy. Therefore during 67–75 s, ESS2 stops working due to fully charged, and the braking energy recovery ability of the ESSs is limited and the rise of substation voltage cannot be suppressed. However, under VCLS, ESS1 recovers most of braking energy during 16–32 s, and they charge simultaneously to satisfy the braking energy recovery requirement in 67–75 s. Therefore, the network voltage is well stabilized. And at 80 s, energy circulates between ESS1 and ESS2 under GA-based strategy. However, under VCLS, ESS1 stops charging, and energy interacts between the powering and braking trains. In summary, VCLS realizes stable learning in MAS, and improves the team profit of the cooperative MG, the experimental results effectively validate the real-time execution of VCLS, during which agents make independent decisions in each time step, realize good cooperation of different SCESSs as well as the trains states, which cannot be implemented by static optimization and single-agent learning. Thereafter, VCLS achieves power deployment optimization of the system through dynamic voltage regulation, and effectively improves utilization of regenerative braking energy.

VI. CONCLUSION

This article proposes and experimentally implements a distributed cooperative control strategy for multiple SCESSs in

urban rail system based on MADRL. The decision process of multi-SCESSs is formulated as a cooperative MG, based on which the multiagent learning framework as well as the hierarchical control structure for individual agent are designed. In simulation studies, energy flow distributions of the traction power system are presented under different strategies, and three indexes are defined to evaluate the energy efficiency of the traction power system. Results show that the proposed VCLS implements stable multiagent learning, and it outperforms the static GA-based strategy in terms of the overall energy saving effect and the braking energy recovery rate. It is because under VCLS, the voltage thresholds are adjusted cooperatively with the train states and SOCs of SCESSs, which effectively optimizes the braking energy allocation between ESSs in different substations, and improves energy transmission of the traction power system. This article presents the first successful attempt to experimentally emulate the operation of dc traction power system with multitrains, substations, and SCESSs based on PHIL, and first attempts to employ the MADRL technology to solve the cooperative control problem of multi-SCESSs along the metro line section. However, due to limited computation sources and experimental equipment for real-time simulation, case studies are based on a medium-scale traction power system with four substations. In the future, we will make efforts to develop this work on a typical metro line with more trains, substations, and SCESSs. Also, this work can be extended to develop an intelligent energy management system that coordinate the operation of multitrains, ESSs, and reversible substations to systematically reduce the energy consumption of urban rail system.

REFERENCES

- [1] A. Gonzlez-Gil, R. Palacin, P. Batty, and J. Powell, "A systems approach to reduce urban rail energy consumption," *Energy Convers. Manage.*, vol. 80, pp. 509–524, 2014.
- [2] M. Khodaparastan, A. A. Mohamed, and W. Brandauer, "Recuperation of regenerative braking energy in electric rail transit systems," *IEEE Trans. Intell. Transp. Syst.*, vol. 20, no. 8, pp. 2831–2847, Aug. 2019.
- [3] X. Yang, X. Li, B. Ning, and T. Tang, "A survey on energy-efficient train operation for urban rail transit," *IEEE Trans. Intell. Transp. Syst.*, vol. 17, no. 1, pp. 2–13, Jan. 2016.
- [4] F. Meishner and D. U. Sauer, "Wayside energy recovery systems in dc urban railway grids," *eTransportation*, vol. 1, 2019, Art. no. 100001.
- [5] S. Vazquez, S. M. Lukic, E. Galvan, L. G. Franquelo, and J. M. Carrasco, "Energy storage systems for transport and grid applications," *IEEE Trans. Ind. Electron.*, vol. 57, no. 12, pp. 3881–3895, Dec. 2010.
- [6] T. Ratniyomchai, S. Hillmansen, and P. Tricoli, "Recent developments and applications of energy storage devices in electrified railways," *IET Electr. Syst. Transp.*, vol. 4, no. 1, pp. 9–20, Mar. 2014.
- [7] A. González-Gil, R. Palacin, and P. Batty, "Sustainable urban rail systems: Strategies and technologies for optimal management of regenerative braking energy," *Energy Convers. Manage.*, vol. 75, pp. 374–388, 2013.
- [8] R. Barrero, X. Tackoen, and J. V. Mierlo, "Improving energy efficiency in public transport: Stationary supercapacitor based energy storage systems for a metro network," in *Proc. IEEE Veh. Power Propulsion Conf.*, Sep. 2008, pp. 1–8.
- [9] F. Ciccarelli, D. Iannuzzi, and I. Spina, "Comparison of energy management control strategy based on wayside ESS for LRV application," in *Proc. 39th Annu. Conf. IEEE Ind. Electron. Soc.*, Nov. 2013, pp. 1548–1554.
- [10] Ivaro J. Lpez-Lpez, R. R. Pecharromn, A. Fernndez-Cardador, and A. P. Cucala, "Assessment of energy-saving techniques in direct-current-electrified mass transit systems," *Transp. Res., Emerg. Technologies*, vol. 38, pp. 85–100, 2014.

- [11] F. Ciccarelli, D. Iannuzzi, K. Kondo, and L. Fratelli, "Line-voltage control based on wayside energy storage systems for tramway networks," *IEEE Trans. Power Electron.*, vol. 31, no. 1, pp. 884–899, Jan. 2016.
- [12] F. Zhu, Z. Yang, H. Xia, and F. Lin, "Hierarchical control and full-range dynamic performance optimization of the supercapacitor energy storage system in urban railway," *IEEE Trans. Ind. Electron.*, vol. 65, no. 8, pp. 6646–6656, Aug. 2018.
- [13] M. Dominguez, A. Fernandez-Cardador, A. P. Cucala, and R. R. Pecharroman, "Energy savings in metropolitan railway substations through regenerative energy recovery and optimal design of ATO speed profiles," *IEEE Trans. Autom. Sci. Eng.*, vol. 9, no. 3, pp. 496–504, Jul. 2012.
- [14] S. Khayyam, F. Ponci, J. Goikoetxea, V. Recagno, V. Bagliano, and A. Monti, "Railway energy management system: Centralized-decentralized automation architecture," *IEEE Trans. Smart Grid*, vol. 7, no. 2, pp. 1164–1175, Mar. 2016.
- [15] N. Zhao, C. Roberts, S. Hillmansen, and G. Nicholson, "A multiple train trajectory optimization to minimize energy consumption and delay," *IEEE Trans. Intell. Transp. Syst.*, vol. 16, no. 5, pp. 2363–2372, Oct. 2015.
- [16] Z. Yang, Z. Yang, H. Xia, F. Lin, and F. Zhu, "Supercapacitor state based control and optimization for multiple energy storage devices considering current balance in urban rail transit," *Energies*, vol. 10, no. 4, 2017, Art. no. 520.
- [17] J. S. Arora, "Introduction to optimum design, 3e," *Probabilistic Eng. Mech.*, vol. 5, no. 2, pp. 100–100, 1990.
- [18] H. Yin, C. Zhao, M. Li, C. Ma, and M.-Y. Chow, "A game theory approach to energy management of an engine-generator/battery/ultracapacitor hybrid energy system," *IEEE Trans. Ind. Electron.*, vol. 63, no. 7, pp. 4266–4277, Jul. 2016.
- [19] H. Chen, R. Ye, X. Wang, and R. Lu, "Cooperative control of power system load and frequency by using differential games," *IEEE Trans. Control Syst. Technol.*, vol. 23, no. 3, pp. 882–897, May 2015.
- [20] X. Zhang, Z. Xu, and T. Yu, "A cyber–physical–social system with parallel learning for distributed energy management of a microgrid," in *Proc. IEEE Innovative Smart Grid Technol. - Asia*, May 2018, pp. 1294–1298.
- [21] S. Su, T. Tang, and C. Roberts, "A cooperative train control model for energy saving," *IEEE Trans. Intell. Transp. Syst.*, vol. 16, no. 2, pp. 622–631, Apr. 2015.
- [22] Q. Gu, T. Tang, F. Cao, and Y. Song, "Energy-efficient train operation in urban rail transit using real-time traffic information," *IEEE Trans. Intell. Transp. Syst.*, vol. 15, no. 3, pp. 1216–1233, Jun. 2014.
- [23] A. Nagabandi, G. Kahn, R. S. Fearing, and S. Levine, "Neural network dynamics for model-based deep reinforcement learning with model-free fine-tuning," in *Proc. IEEE Int. Conf. Robot. Automat.*, 2018, pp. 7559–7566.
- [24] D. Silver, T. Hubert, J. Schrittwieser, I. Antonoglou, and D. Hassabis, "A general reinforcement learning algorithm that masters chess, shogi, and go through self-play," *Science*, vol. 362, no. 6419, pp. 1140–1144, 2018.
- [25] D. Zhang, X. Han, and C. Deng, "Review on the research and practice of deep learning and reinforcement learning in smart grids," *CSEE J. Power Energy Syst.*, vol. 4, no. 3, pp. 362–370, Sep. 2018.
- [26] T. T. Nguyen, N. D. Nguyen, and S. Nahavandi, "Deep reinforcement learning for multi-agent systems: A review of challenges, solutions and applications," 2018, *arXiv:1812.11794*.
- [27] P. Hernandez-Leal, B. Kartal, and M. E. Taylor, "A survey and critique of multiagent deep reinforcement learning," *Auton. Agents and Multi-Agent Syst.*, vol. 33, no. 6, Oct. 2019, Art. no. 750797. [Online]. Available: <http://dx.doi.org/10.1007/s10458-019-09421-1>
- [28] G. Palmer, K. Tuyls, D. Bloembergen, and R. Savani, "Lenient multi-agent deep reinforcement learning," in *Proc. 17th Int. Conf. Auton. Agents and MultiAgent Syst.*, 2018, pp. 443–451.
- [29] J. Foerster, N. Nardelli, G. Farquhar, P. H. S. Torr, P. Kohli, and S. Whiteson, "Stabilising experience replay for deep multi-agent reinforcement learning," in *Proc. 34th Int. Conf. Mach. Learning*, 2017, pp. 1146–1155.
- [30] R. Lowe, Y. Wu, A. Tamar, J. Harb, O. P. Abbeel, and I. Mordatch, "Multi-agent actor-critic for mixed cooperative-competitive environments," in *Proc. Adv. Neural Inf. Process. Syst.*, 2017, pp. 6379–6390.
- [31] P. Sunehag *et al.*, "Value-decomposition networks for cooperative multi-agent learning based on team reward," in *Proc. 17th Int. Conf. Auton. Agents and Multiagent Syst.*, 2018, pp. 2085–2087.
- [32] *Train Operation Calculation and Design*. Beijing, China: People's Transportation Press, 2008.
- [33] H. Aziz, "Multiagent systems: Algorithmic, game-theoretic, and logical foundations by Y. Shoham and K. Leyton-brown Cambridge University Press, 2008," *ACM Sigact News*, vol. 41, no. 1, pp. 34–37, 2010.
- [34] F. A. Oliehoek and C. Amato, *A Concise Introduction to Decentralized POMDPs*. New York, NY, USA: Springer, 2016.
- [35] M. Ruiz-Corts *et al.*, "Optimal charge/discharge scheduling of batteries in microgrids of prosumers," *IEEE Trans. Energy Convers.*, vol. 34, no. 1, pp. 468–477, Mar. 2019.
- [36] V. I. Herrera, H. Gaztaaga, A. Milo, A. Saez-de-Ibarra, I. Etxeberria-Otadui, and T. Nieva, "Optimal energy management of a battery-supercapacitor based light rail vehicle using genetic algorithms," in *Proc. IEEE Energy Convers. Congr. Expo.*, Sep. 2015, pp. 1359–1366.
- [37] H. Xia, H. Chen, Z. Yang, F. Lin, and B. Wang, "Optimal energy management, location and size for stationary energy storage system in a metro line based on genetic algorithm," *Energies*, vol. 8, no. 10, pp. 11618–11640, 2015.
- [38] A. Chipperfield, P. Fleming, H. Pohlheim, and C. Fonseca, "Genetic algorithm toolbox for use with MATLAB, version 1.2," Dept. Autom. Control Syst. Eng., Univ. Sheffield, Sheffield, U.K., 1994.
- [39] M. D. Omar Faruque *et al.*, "Real-time simulation technologies for power systems design, testing, and analysis," *IEEE Power Energy Technol. Syst. J.*, vol. 2, no. 2, pp. 63–73, Jun. 2015.



Feiqin Zhu (Student Member, IEEE) received the B.S. degree in electrical engineering from Beijing Jiaotong University, Beijing, China, in 2015. She is currently working toward the Ph.D. degree in electrical engineering with the School of Electrical Engineering, Beijing Jiaotong University, Beijing, China.

Her research interests include modeling and optimization of energy storage systems, cooperative control, and energy management in urban railway.



Zhongping Yang (Member, IEEE) received the B.Eng. degree in electrical engineering from the Tokyo University of Mercantile Marine, Tokyo, Japan, in 1997, and the M.Eng. and Ph.D. degrees in electrical engineering from the University of Tokyo, Tokyo, Japan in 1999 and 2002, respectively.

He is currently a Professor with the School of Electrical Engineering, Beijing Jiaotong University, Beijing, China. His research interests include high-speed rail integration technology, traction & regenerative braking technology, and wireless power transfer of urban rail vehicles.

Prof. Yang received the Zhan Tianyou Award for Science and Technology in 2010, the Excellent Popular Science and Technology Book Award in 2011, and the Science and Technology Progress Award (second prize) of the Ministry of Education in China in 2016.



Fei Lin (Member, IEEE) received the B.S. degree in electrical engineering from Xi'an Jiaotong University, Xi'an, China, in 1997; the M.S. degree in electrical engineering from Shandong University, Jinan, China, in 2000; and the Ph.D. degree in electrical engineering from Tsinghua University, Beijing, China, in 2004.

He is currently a Professor with the School of Electrical Engineering, Beijing Jiaotong University, Beijing. His research interests include traction converter and motor drives, energy management for railway systems, and digital control of power-electronic-based devices.



Yue Xin (Student Member, IEEE) received the B.S. degree in electrical engineering in 2017, from Beijing Jiaotong University, Beijing, China, where is currently working toward the master's degree in electrical engineering with the School of Electrical Engineering.

Her research interests include characteristic test of supercapacitor cells and optimization of energy management strategy for energy storage systems in urban railway.